minerals

MDPI

Communication

First Detection of Methane within Chromitites of an Archean-Paleoproterozoic Greenstone Belt in Brazil

Yuri de Melo Portella [1,2,*], Federica Zaccarini [3] and Giuseppe Etiope [4]

[1] Programa de Pós-Graduação em Geociências (PPGGEO), Universidade Federal do Rio Grande do Sul (UFRGS), Av. Bento Gonçalves, 9500, Porto Alegre, RS 91501-970, Brazil
[2] Exploration, Petrobras S.A., Av. República do Chile, 330, Rio de Janeiro, RJ 20031-170, Brazil
[3] Department Angewandte Geowissenshaften und Geophysik, Montanuniversität Leoben, Peter Tunner Str. 5, A-8700 Leoben, Austria; federica.zaccarini@unileoben.ac.at
[4] Istituto Nazionale di Geofisica e Vulcanologia, Sezione Roma 2, via V. Murata 605, 00143 Roma, Italy; giuseppe.etiope@ingv.it
* Correspondence: yuri_portella@hotmail.com; Tel.: +55-19-991080987

Received: 5 April 2019; Accepted: 26 April 2019; Published: 29 April 2019

Abstract: Abiotic methane is widely documented in seeps, springs and aquifers associated with mafic-ultramafic rocks in Phanerozoic ophiolites, peridotite massifs and intrusions worldwide. Chromitites in ophiolites, in particular, have been interpreted as the rocks potentially generating methane though CO_2 hydrogenation. Here, we document, for the first time, the presence of methane within chromitites in South America. We analyzed, through milling and gas extraction, the content of gas occluded in Cedrolina chromitite samples, belonging to the Pilar de Goiás greenstone belt in Brazil. The chromitites display significant gas concentrations up to 0.31 μg CH_4/g_{rock} and 2800 ppmv of hydrogen, while the host talc schist is devoid of gas. Stable C isotope composition of methane ($\delta^{13}C$ from −30 to −39.2‰) and the absence of organic-matter rich metasediments in the region suggest an abiotic origin. Hydrogen and methane concentrations appear related to high-Cr chromite modal content and to the presence of Ni-sulfides/alloys, which are potential catalysts of CO_2 hydrogenation at temperatures above 200 °C. Accessory ruthenium-bearing minerals occurring in the chromitites could also act as catalysts, even at lower temperatures. Geothermometry of chlorite found in the chromitites constrains serpentinization at ~250 °C, during lower greenschist facies retrometamorphism. Hydrogen could be autochthonous, and thus formed under similar temperature, which we hypothesize represents the upper limit for abiotic methane generation in the area (250 °C). The Cedrolina chromitites are the first example of CH_4 occurrence in ultramafic rocks related to an Archean-Paleoproterozoic greenstone belt. This may imply that serpentinized Cr-rich chromitites could have been sources of methane for the early Earth's atmosphere.

Keywords: chromite; catalysts; Ni-sulfides; Ni-Fe alloys; abiotic methanogenesis; serpentinization; hydrogen; chlorite geothermometry; Pilar de Goiás greenstone belt

1. Introduction

The abiotic synthesis of methane (CH_4) after serpentinization of ultramafic rocks has long been documented, often associated with considerable amounts of hydrogen (H_2), both in hydrothermal mid-ocean ridge submarine environments and in continental serpentinization sites [1–3]. In hydrothermal submarine environments, serpentinization of peridotitic rocks is driven by seawater under relatively high temperatures (>200 °C; e.g., [3,4]). Conversely, continental serpentinization is driven by meteoric water at lower temperatures, typically below 150 °C [5,6]. On continents, methane with a dominant abiotic origin has been discovered in Phanerozoic ophiolites, peridotite massifs and intrusions in at

least 18 countries distributed over Europe, the Middle East, Asia, Oceania and North America [2]. Methane observed in Precambrian shields (e.g., [7]) could also have a similar abiotic origin. Abiotic methanogenesis has implications on the origin of life [8], its potential occurrence on Mars and other planets [9–11], and in igneous reservoir rocks [2,7,12–14].

Inorganic methane formation is widely linked to metal-catalysed Fischer–Tropsch-type (FTT) synthesis in serpentinized ultramafic rocks, especially the Sabatier reaction ($4H_2 + CO_2 = CH_4 + 2H_2O$), also known as carbon dioxide hydrogenation or methanation [2,4,15,16]. Molecular hydrogen necessary for methanation can be sourced by serpentinization (i.e., hydration) of olivine and pyroxene, which leads to ferrous iron oxidation and secondary Fe-bearing minerals like magnetite, serpentine and chlorite [17,18]. Hydrogen formation is favoured when H_2O molecules and/or Fe^{2+} from dissolved silicates adsorb onto spinel surfaces, participating in interfacial electron transfer and resulting in sustained reduction of water even at low temperatures [19]. Carbon dioxide, instead, may have various sources, including the mantle, limestones and the atmosphere [2].

Among the most common catalysts for CO_2 hydrogenation are magnetite, Fe-Ni alloys and chromium, which also buffer reducing conditions [20]. In addition, experimental serpentinization of komatiites has led [21] to deduce that Ni-sulfides may as well be important catalysts for hydrothermal abiotic methanogenesis. Further experimental data demonstrated that also ruthenium (Ru), a Platinum Group Element (PGE), can act as catalyst in the formation of abiotic methane at low temperatures (<150 °C) [15]. Moreover, [22] documented that, among the various ophiolite lithotypes in Greece, only high chromium and ruthenium chromitites host significant amounts of methane, hydrogen and heavier hydrocarbons, having therefore been interpreted as source rocks of abiotic methane.

Here we present preliminary data on the occurrence of methane associated with chromitites of an Archean-Paleoproterozoic greenstone belt in South America. We have analyzed the gas occluded in the Cedrolina chromitite, belonging to the Pilar de Goiás greenstone belt, in Brazil. The Cedrolina chromitite, either part of a Precambrian ophiolite or a stratiform intrusion, is a poly-metamorphosed ultramafic body hosting sub economic concentrations of PGE and Minerals (PGM), such as irarsite and laurite [23]. In addition to analyses of gas occluded in the rock, microanalysis and geothermometry of chlorite inclusions in chromite and in the Cedrolina chromitite's matrix were carried out to estimate serpentinization temperature, as well as the retrometamorphic greenschist facies conditions for the area. Such parameters could help constrain the timing and temperature for optimum H_2 production and provide an upper limit for methanation temperature.

2. General Geology

The Cedrolina chromitite is part of a mafic-ultramafic formation of the Pilar de Goiás greenstone belt (PGGB), located in the Tocantins Province, central Brazil. The Tocantins Province comprises of the Brasília, Paraguai and Araguaia supracrustal fold belts that resulted from the Neoproterozoic collage of West Gondwana [24,25] (Figure 1A). Within the Brasilia Belt, the Archean-Paleoproterozoic Terrane of Goiás is considered an allochthonous block which was amalgamated during the late stages of the Brasiliano/Pan-African orogeny [25]—Figure 1B. In the northern section of the Terrane, an association of Archean orthogneissic complexes is tectonically juxtaposed with irregularly shaped ~N–S elongated Archean-Paleoproterozoic greenstone belts (Crixás, Guarinos and Pilar de Goiás from West to East, respectively) ([26] and references therein)—Figure 1B.

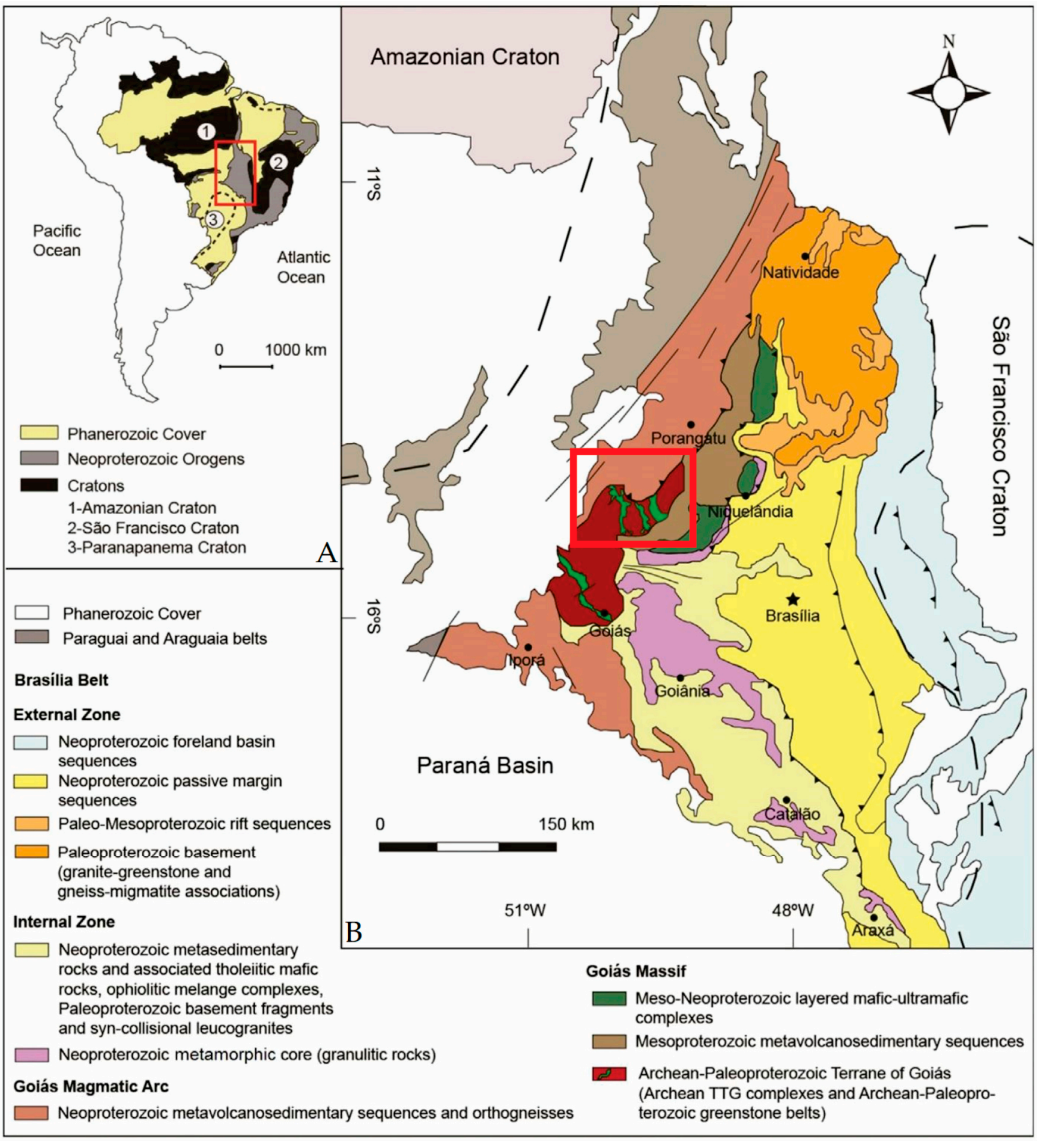

Figure 1. (**A**) Major geological units of Brazil represented by undivided Phanerozoic cover (basins), Neoproterozoic Orogens (fold belts) and Cratons. Location of the Tocantins Province in Central Brazil is highlighted by the red rectangle. (**B**) Highlighted area in (**A**) showing the Brasília Fold Belt units and the allochthonous Archean-Paleoproterozoic Terrane of Goiás in its western edge (modified after [26,27]). Red rectangle features the northern section of the Terrane, in which light green stripes represent the ~N-S trending greenstone belts of Crixás, Guarinos and Pilar de Goiás (from W-E), while maroon color stands for adjacent Archean TTG complexes (tonalite-trondhjemite-granodiorite orthogneisses).

PGGB consists of a greenschist [28] to amphibolite facies [29] metavolcanosedimentary sequence. The lower units, to the East, are characterized by metakomatiites (Córrego Fundo Formation) and metabasalts (Cedrolina Formation) with minor intercalated metacherts and banded iron formations (BIF). The upper units, to the West, are formed by metacherts, calcsilicates and marbles of the Boqueirão Formation and metapelites from the Serra do Moínho Formation [30]. In the northern portion of the PGGB, [23] estimated that the metamorphic peak for the Cedrolina chromitites (Figures 1B and 2) reached the low amphibolite facies (550–600 °C at 0.4–0.6 GPa), which was followed by retrometamorphism under greenschist facies conditions. Although the number of tectono-metamorphic events and their specific ages is not a consensus, four deformational stages have been suggested for the analogous Crixás Belt [31], two during the Paleoproterozoic (including the main event) and two in the Neoproterozoic.

The Cedrolina Chromitite

The Cedrolina chromitite was studied in great detail by [23,32]. Those authors describe it as a tabular, ~1.5 m thick, elliptical (230 × 100 m) body concordantly emplaced within the lower mafic–ultramafic metavolcanic rocks of the Cedrolina Formation, which is hosted by talc schists (Figure 2). Although not observed in situ due to intense deformation, weathering and reduced number of outcrops, in some boulders sharp to graded contacts are visible between the chromitite and the host rock (Figure 3). The talc schist is composed mainly of talc (90%), chromite (<5%), hydrated Al-silicates (3%) and magnetite + Fe-hydroxide pseudomorphs after magnetite (2%) (Figure 3B).

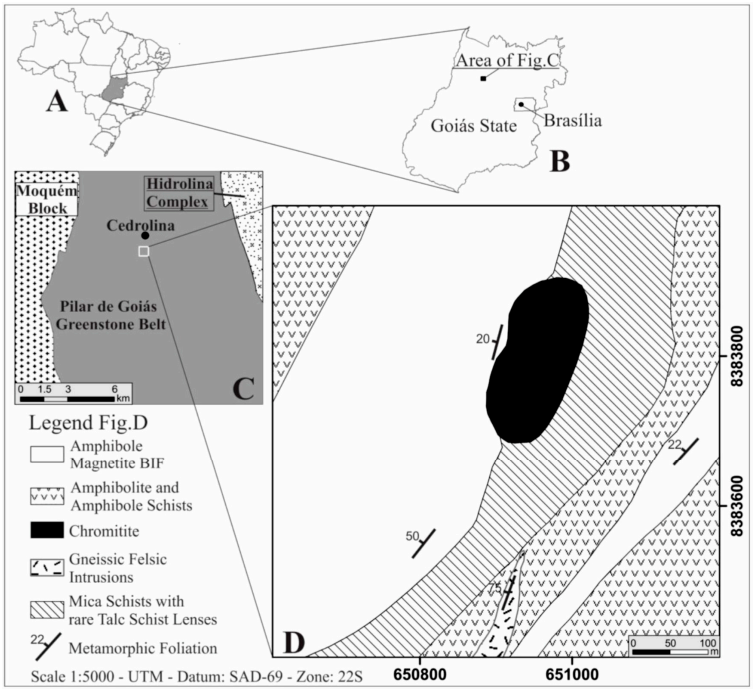

Figure 2. Geological sketch maps of Cedrolina chromitites (**A**,**B**) Geographical location of the studied area; (**C**) General geology of the central-northern Pilar de Goiás greenstone belt area simplified after [33]; (**D**) Detailed geological map of a small portion of the Cedrolina Formation where the investigated chromitites occur (after [23,32]).

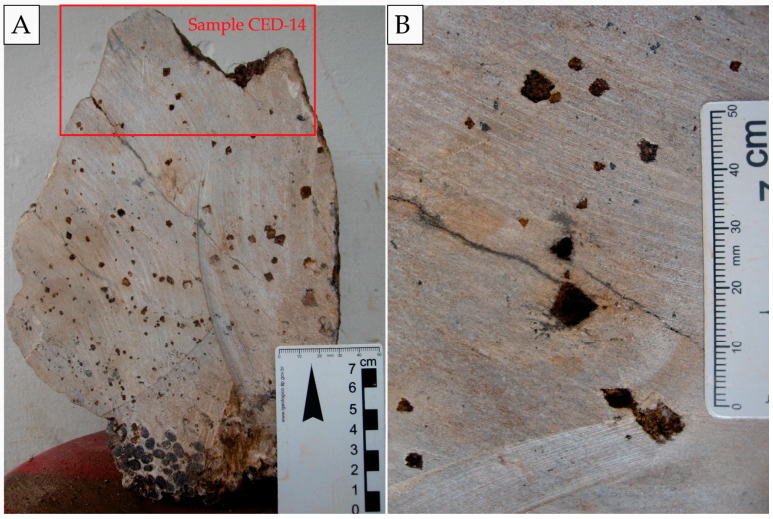

Figure 3. (**A**) Sharp contact between the host talc schist (above) and nodular chromitite (in the bottom) observed in loose boulder. The metamorphic foliation is approximately perpendicular to the contact.

Note abundant Fe-hydroxide pseudomorphs after spinel. Red rectangle indicates where sample CED-14 was acquired; (**B**) Detail of Fe-hydroxide pseudomorphs after magnetite octahedra found in the host talc schist. Some of them are only partially filled, characterizing secondary porosity.

Macroscopically the chromitite ore is characterized by a peculiar nodular structure, consisting of rounded (~1 cm diameter) massive to intensely fractured orbs (Figure 4) immersed in a matrix of platy chlorite and talc that define a strong NW-dipping schistosity. Fractures are mostly filled with chlorite or talc, and rarely rutile. The mean modal mineralogy of the chromitite is made up of 60% chromite, 25% talc and 15% Cr-rich chlorite, with traces up to few percentages of iron hydroxides and rutile. Among recognized accessory minerals in the matrix or included in chromite are Ce-monazite (Ce,La,Nd,Pr,Th)PO_4 [34], zircon, arsenopyrite, chalcopyrite, sphalerite, heazlewoodite (Ni_3S_2), argentite (Ag_2S), magnetite, thorianite (ThO_2), uraninite (UO_2), native gold, noble metal alloys, irarsite ((Ir,Ru,Rh,Pt)AsS) and laurite (RuS_2) [23].

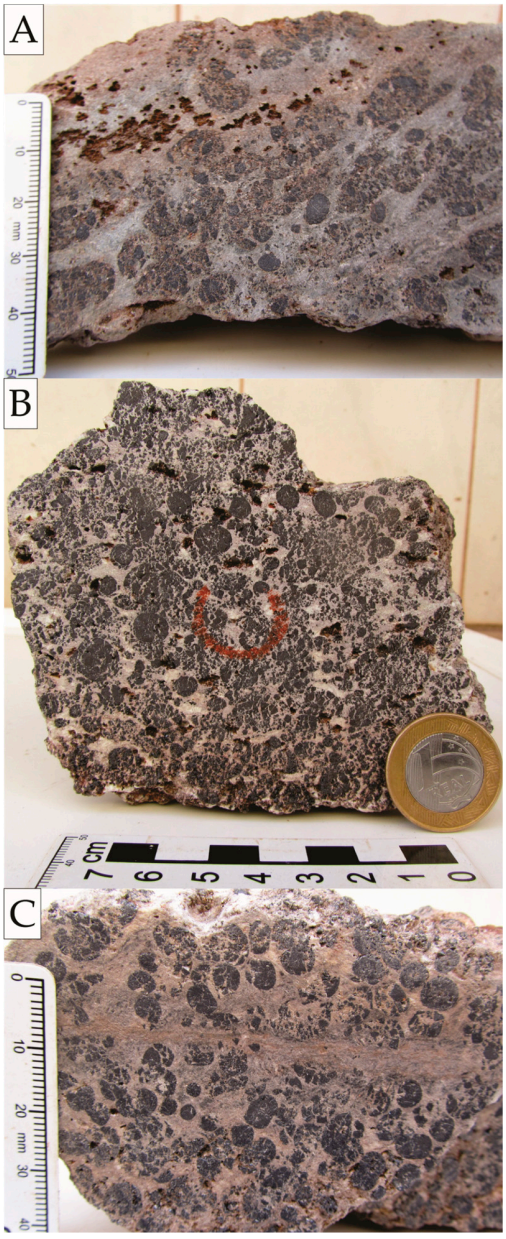

Figure 4. Hand samples of the analyzed chromitites displaying massive to intensely fractured orbs of chromite immersed in a silicate matrix. Apparent porosity is mostly due to mechanical ablation of minerals

during sawing and sample preparation, however, some secondary porosity is observed where spinels are oxidized. (**A**) Sample CED-106A2 displaying a greenish matrix and some secondary porosity associated with Fe-hydroxides pseudomorphs (least weathered); (**B**) Sample CED-47C showing a whitish-gray matrix (mildly weathered); (**C**) Sample CED-105B is characterized by a yellowish-gray matrix and increased friability due to its high weathering stage.

Microprobe analyses of chromite indicate an average high Cr (55 wt%), Fe (FeO 27 wt%; Fe_2O_3 6 wt%) and MnO (>0.7 wt%) concentration, while Al_2O_3 (7 wt%), MgO (3.8 wt%), TiO_2 (0.2 wt%) and V_2O_3 (0.15 wt%) are less abundant [23]. Chlorite is characterized by high MgO (av. 30 wt%) and very high Cr_2O_3 (av. >3.23 wt%) contents, occurring in the matrix or as inclusions in chromite which are frequently oriented [23,32] (Figure 5).

The Cedrolina chromitites and their country rocks were affected by a strong poly-metamorphic overprint and intense weathering. Therefore, it was impossible to establish their original nature, i.e., podiform or stratiform, as well as the geodynamic setting, a Precambrian ophiolite or intrusion, in which they formed [23].

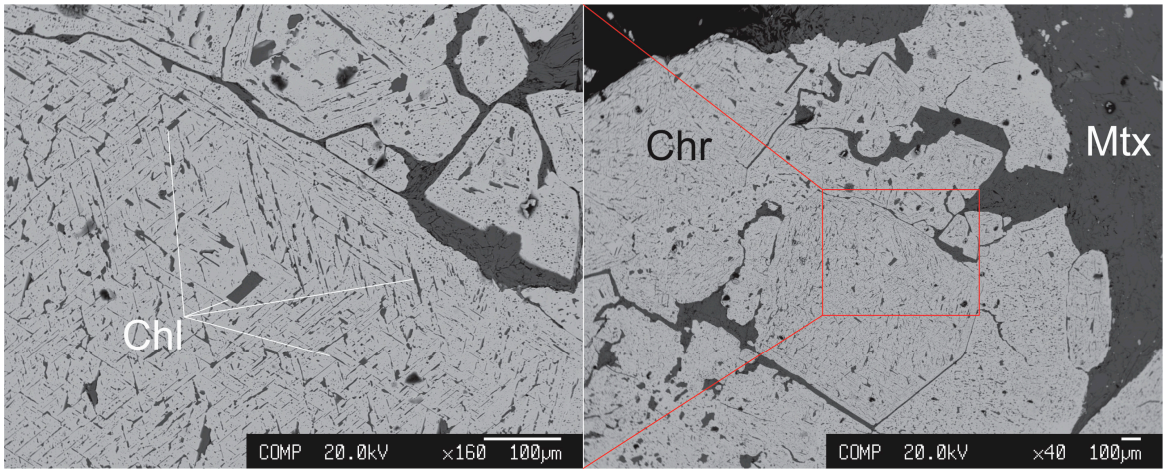

Figure 5. Backscattered electron images of abundant oriented Cr-rich chlorite inclusions in chromite (Sample CED-105) [32]. Abbreviations: Chl = chlorite; Chr = chromite; Mtx = matrix.

3. Materials and Methods

Four samples of the Cedrolina chromitites, selected on the basis of the different weathering stages, and one host rock (talc schist) were investigated for their gas content, following the procedure adopted in [22]. In brief, rock samples were crushed into 1 cm chips and successively milled by planetary ball mill for 3 min at 400 rounds per minute. The content of CH_4 and H_2 in the gas extracted in the grinding jar was then analyzed via TDLAS (tunable diode laser absorption spectroscopy) CH_4 sensor (GAZOMAT, mounted in a West Systems sensor package; range 0.1 ppmv–100%v/v; repeatability 0.1 ppmv), and semiconductor H_2 sensor (Huberg; range 0–5000 ppmv; repeatability 5 ppmv). Gas was then transferred from the jar into 0.25 or 0.5 L Teflon bags for stable C isotope analyses of CH_4 by Cavity Ring-Down Spectroscopy (Picarro G2112-I CH_4 isotope analyzer, precision <0.8‰ at 20 ppmv CH_4, 5 min, 1σ, based on two standards with $\delta^{13}C$: −20‰ and −40‰ VPDB). The same procedure was applied to six "blank" rocks (granite, quartz and limestone), considered to be gas-free (see details in [22]).

Quantitative wavelength dispersive spectrometer (WDS) electron microprobe analyses of chlorite were carried out at the Eugen F. Stumpfl laboratory (Leoben University, Leoben, Austria), using a Jeol JXA 8200 Superprobe, Tokyo, Japan). The same instrument was used to obtain electronic images. Chlorite was quantitatively analyzed with 15 kV of accelerating voltage and 10 nA of beam current. All the elements were analyzed using the Kα line, and were calibrated on natural chromite, rhodhonite, ilmenite, wollastonite, kaersutite, olivine, millerite, and sanidine. The following diffracting crystals

were used: TAP for Mg, Al and Na, PETJ for Si, K and Ca, and LIFH for Ti, Cr, Mn, Ni, and Fe. The counting times for peak and background were 20 and 10 s respectively.

4. Results

The analyses of gas content inside the rocks are summarized in Table 1 and Figure 6. The chromitites display significant methane concentrations, exceeding 0.3 μg CH_4/g_{rock} in the most weathered sample (CED-105B). The freshest sample (CED-106A2) displayed lower methane concentration. The chromitite's host rock (CED-14) is almost devoid of CH_4, with values comparable to blanks (Figure 6). High hydrogen levels (>2800 ppmv in the extracted gas phase) were also detected in the same chromitites with higher CH_4 content (CED-47C and CED-105B), while samples CED-106A2 and CED-14 (talc schist) present values 2–3 orders of magnitude lower (in the same range of blanks). The very low concentrations of methane and hydrogen in blank samples can be attributed to milling artefacts [22].

Table 1. Concentration of CH_4, H_2 and stable C isotopic ratio of CH_4 in the gas extracted from Cedrolina samples. The main mineralogical data for each sample are also shown.

Sample (CED)	14	106A2	47C	105B	105B
Rock Type	talc schist *	chromitite	chromitite	chromitite	chromitite
Weathering Stage	mild	low	mild	strong	strong
Chromite's Modal Content in the rock	<5%	20–30%	50–60%	40–50%	40–50%
Accessory Minerals	Mag	Apy; Ccp; Gn; Pn; Pyr;	Apy; Sp; Pyr; AsS; Hw; Arg; Mag	Apy; Hw; Aw	Apy; Hw; Aw
Weight (g)	140	160	270	270	190
CH_4 ppmv	2	32	434	610	612
CH_4 (μg/g_{rock})	0.002	0.020	0.124	0.175	0.306
H_2 ppmv	5	12	2830	>4500	50
δ^{13}C-CH_4 (‰ VPDB)			−39.2		−30

* host of the chromitites; Empty cells means "not measured"; Abbreviations: Apy = arsenopyrite, Arg = argentite (Ag_2S), AsS = Arsenium sulfide, Aw = awaruite ($Ni_{2-3}Fe$), Ccp = chalcopyrite, Gn = galena, Hw = heazlewoodite (Ni_3S_2), Mag = magnetite, Pn = pentlandite, Pyr = pyrite/pyrrhotite, Sp = sphalerite.

We observe a correlation between methane content and modal chromite abundance. Samples with CH_4 exceeding 0.1 μg CH_4/g_{rock} (CED-47C and 105B) have >40% modal chromite and contain accessory heazlewoodite (Ni_3S_2), plus awaruite ($Ni_{2-3}Fe$) only in sample 105B. Conversely, sample CED-106A2, with the lowest CH_4 content, has a modal chromite abundance of 20–30% and is devoid of heazlewoodite and awaruite.

Carbon isotope analyses of CH_4 from samples CED-47C and CED-105B display a $\delta^{13}C$ signature ranging from −30 to −39.2‰ (Table 1). This range is compatible with both a thermogenic (biotic) and abiotic origin [2].

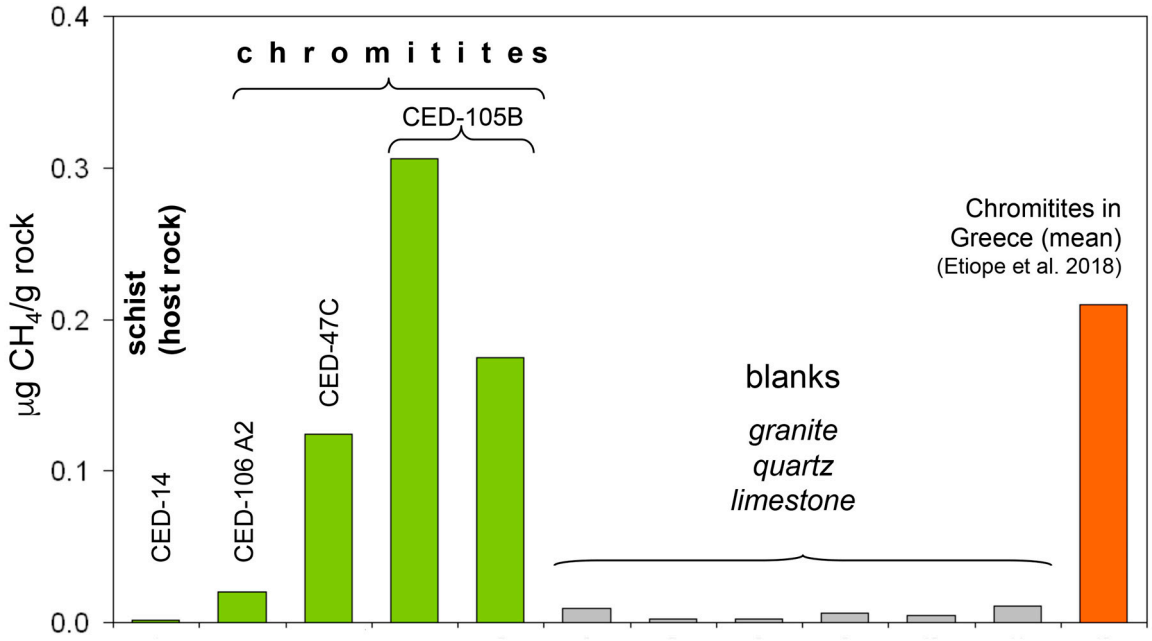

Figure 6. Methane content in the Cedrolina (CED) samples compared with blank rock samples and the average CH_4 content in chromitites of greek ophiolites reported by [22].

Chlorite Microanalyses and Geothermometry

It is well known that the compositional variations of chlorite can reflect physicochemical conditions in which the mineral was formed [35–38]. In particular, the amount of ^{IV}Al substituting Si in the tetrahedral site is believed to be controlled by temperature. Therefore, different geothermometric equations based on this substitution [35,36] have been applied to evaluate the metamorphism temperature associated with chlorite formation in the Cedrolina chromitite. Calculated temperatures for matrix chlorite and inclusions in chromite both present mean values of 240–275 °C and their thermometric significance was not affected by alkalis contamination [39], being the values of Ca + Na + K (at%) less than 0.1 (Table 2).

Table 2. Chlorite electron microprobe data and geothermic calculations.

(wt%)	Sample (CED)	SiO_2	TiO_2	Al_2O_3	FeO	MnO	MgO	CaO	Na_2O	K_2O	Cr_2O_3	NiO	Total
Matrix	105C.10	28.60	0.02	18.26	1.79	0.07	29.95	0.01	0.00	0.03	4.33	0.32	83.37
	105C.2	29.52	0.02	17.06	2.26	0.10	31.21	0.00	0.02	0.00	3.30	0.31	83.80
	105C.4	28.62	0.04	18.87	2.30	0.05	30.22	0.01	0.07	0.04	3.40	0.38	83.99
	105C.5	29.93	0.04	16.43	1.84	0.00	30.10	0.02	0.05	0.05	3.87	0.31	82.63
	105C.7	29.25	0.03	18.03	2.54	0.04	29.40	0.01	0.08	0.03	3.96	0.28	83.65
	105C.8	30.02	0.02	15.98	2.17	0.02	30.90	0.04	0.04	0.04	3.95	0.34	83.52
	105C.9	30.26	0.02	16.29	2.11	0.04	31.87	0.00	0.03	0.03	3.62	0.32	84.59
	106D.1	31.70	0.05	17.60	4.10	0.11	27.99	0.12	0.04	0.16	2.13	0.22	84.23
	106D.10	31.15	0.07	17.35	3.78	0.00	29.79	0.05	0.03	0.18	2.10	0.08	84.56
	106D.3	33.26	0.04	20.68	3.02	0.07	23.89	0.07	0.02	0.13	1.97	0.22	83.38
	106D.6	32.10	0.07	17.92	3.94	0.01	29.25	0.14	0.03	0.19	1.99	0.22	85.85
	106D.7	32.06	0.04	19.22	3.51	0.01	28.19	0.02	0.01	0.09	2.19	0.25	85.57
	106D.8	29.86	0.01	20.30	4.02	0.06	27.43	0.07	0.01	0.02	2.47	0.22	84.48
Included in Chr	105Cin2	29.81	0.02	17.35	1.81	0.01	29.51	0.02	0.08	0.04	4.43	0.31	83.38
	105Cin3	31.80	0.02	16.58	1.62	0.01	30.73	0.05	0.01	0.03	3.83	0.30	84.95
	105Cin4	30.67	0.04	17.66	1.76	0.00	30.22	0.01	0.05	0.07	4.05	0.30	84.83
	105Cin5	29.63	0.03	16.89	1.57	0.02	30.60	0.04	0.04	0.02	4.08	0.30	83.22
	105Cin6	30.54	0.01	16.71	1.53	0.05	31.49	0.01	0.01	0.01	3.88	0.31	84.57
	105Cin8	28.65	0.04	18.87	1.92	0.08	30.02	0.06	0.03	0.02	3.20	0.37	83.26
	105Cin9	31.04	0.04	17.63	1.63	0.05	31.17	0.02	0.00	0.03	3.88	0.38	85.86
	106A1in1	29.63	0.05	19.69	6.97	0.03	28.71	0.04	0.00	0.06	1.90	0.18	87.26
	106Din1	30.76	0.03	19.22	3.91	0.12	30.07	0.00	0.02	0.11	3.02	0.19	87.44
	106Din2	29.92	0.04	17.83	4.03	0.09	31.13	0.04	0.07	0.04	2.92	0.13	86.24
	106Din4	30.56	0.04	17.31	3.43	0.04	28.09	0.21	0.13	0.04	2.68	0.21	82.72

Table 2. *Cont.*

														Calculated T (°C)			
(at%)		**Si**	**Ti**	**Al$^{(IV)}$**	**Al$^{(VI)}$**	**Fe**	**Mn**	**Mg**	**Ca**	**Na**	**K**	**Cr**	**Ni**	**Fe#**	**1**	**2**	**3**	**4**
Matrix	105C.10	5.65	0.00	2.35	1.91	0.30	0.01	8.83	0.00	0.00	0.01	0.68	0.10	0.03	267	316	269	295
	105C.2	5.80	0.00	2.20	1.76	0.37	0.02	9.15	0.00	0.01	0.00	0.51	0.10	0.04	251	292	254	279
	105C.4	5.62	0.01	2.38	1.98	0.38	0.01	8.84	0.00	0.03	0.01	0.53	0.12	0.04	271	322	274	299
	105C.5	5.95	0.01	2.05	1.80	0.31	0.00	8.92	0.00	0.02	0.01	0.61	0.10	0.03	235	268	238	264
	105C.7	5.77	0.00	2.23	1.97	0.42	0.01	8.65	0.00	0.03	0.01	0.62	0.09	0.05	254	297	258	281
	105C.8	5.93	0.00	2.07	1.64	0.36	0.00	9.10	0.01	0.02	0.01	0.62	0.11	0.04	238	272	241	266
	105C.9	5.89	0.00	2.11	1.63	0.34	0.01	9.25	0.00	0.01	0.01	0.56	0.10	0.04	241	277	244	270
	106D.1	6.20	0.01	1.80	2.26	0.67	0.02	8.16	0.03	0.02	0.04	0.33	0.07	0.08	209	228	215	233
	106D.10	6.08	0.01	1.92	2.07	0.62	0.00	8.67	0.01	0.01	0.04	0.32	0.02	0.07	222	248	227	247
	106D.3	6.45	0.01	1.55	3.18	0.49	0.01	6.91	0.01	0.01	0.03	0.30	0.07	0.07	182	188	187	208
	106D.6	6.15	0.01	1.85	2.20	0.63	0.00	8.36	0.03	0.01	0.05	0.30	0.07	0.07	214	235	219	239
	106D.7	6.13	0.01	1.87	2.46	0.56	0.00	8.04	0.00	0.00	0.02	0.33	0.08	0.07	216	239	221	242
	106D.8	5.83	0.00	2.17	2.50	0.66	0.01	7.98	0.01	0.00	0.00	0.38	0.07	0.08	248	288	254	273
Included in Chr	105Cin2	5.80	0.00	2.20	1.76	0.37	0.02	9.15	0.00	0.01	0.00	0.51	0.10	0.04	251	292	254	279
	105Cin3	6.12	0.00	1.88	1.88	0.26	0.00	8.82	0.01	0.00	0.01	0.58	0.09	0.03	217	240	219	246
	105Cin4	5.93	0.01	2.07	1.96	0.28	0.00	8.71	0.00	0.02	0.02	0.62	0.09	0.03	237	271	240	266
	105Cin5	5.85	0.00	2.15	1.78	0.26	0.00	9.01	0.01	0.02	0.01	0.64	0.09	0.03	246	284	248	275
	105Cin6	5.93	0.00	2.07	1.75	0.25	0.01	9.11	0.00	0.00	0.00	0.60	0.10	0.03	238	272	240	267
	105Cin8	5.65	0.01	2.35	2.04	0.32	0.01	8.83	0.01	0.01	0.00	0.50	0.12	0.03	267	316	269	295
	105Cin9	5.92	0.01	2.08	1.89	0.26	0.01	8.87	0.00	0.00	0.01	0.58	0.12	0.03	238	272	240	267
	106A1in1	5.70	0.01	2.30	2.16	1.12	0.00	8.23	0.01	0.00	0.01	0.29	0.05	0.12	262	308	271	282
	106Din1	5.82	0.00	2.18	2.11	0.62	0.02	8.49	0.00	0.01	0.03	0.45	0.06	0.07	248	288	254	274
	106Din2	5.77	0.01	2.23	1.82	0.65	0.01	8.95	0.01	0.03	0.01	0.44	0.04	0.07	254	297	259	280
	106Din4	6.09	0.01	1.91	2.15	0.57	0.01	8.34	0.05	0.05	0.01	0.42	0.07	0.06	221	246	226	247
	Mean														**238**	**273**	**242**	**266**
	Median														**240**	**275**	**242**	**268**

Fe# = Fe/(Fe+Mg); Calculated temperatures based on different equations: 1 = [35]; 2 = [37]; 3 = [36]; 4 = [38].

5. Discussion

Petrography and microprobe analyses of the studied samples suggest that their mineralogy may influence the gas content of the rocks. Notably, chromite's modal content and the presence of Ni-sulfides/alloys seem to control H_2 and CH_4 abundances. Besides having the lowest chromite modal percentage (20–30%), hydrogen and methane concentration, sample CED-106A2 is also the least weathered among all chromitite samples. Conversely, samples CED-47C and 105B represent increasing weathering stages, as well as increasing methane concentration (Figure 6). In addition, both samples have accessory heazlewoodite (as already described in [23]), a nickel rich sulfide, while awaruite ($Ni_{2\text{-}3}Fe$) was only encountered in sample 105B (Table 1). Thus, we hypothesize that awaruite could be a more efficient Sabatier catalyst than heazlewoodite. In the Cedrolina chromitites, small amounts of micrometer sized ruthenium-bearing minerals like laurite and irarsite described by [23] could also favor low-T (<150 °C) CO_2 hydrogenation as suggested by [15,22].

Supergene weathering is understood here as a near-surface liquid water-rock interaction (<100 °C at 1 atm) which is responsible for hydration/oxidation of the mineral assemblage and soil formation. Such regional processes of lateritization and pedogenesis, observed both macro and microscopically, lead to spinel oxidation into Fe-hydroxides, silicate decomposition into Mg and Al-hydroxides and an overall change in matrix color from greenish to yellowish/reddish. Associated secondary porosity is regarded as exclusive of tropical weathering conditions, assuming that plutonic and metamafic rocks have negligible primary porosity and permeability.

The paucity of methane and hydrogen (2 and 5 ppmv, respectively) in the talc schist (CED-14) surrounding the chromitite strongly suggests that both gases are autochthonous and formed within the chromite-rich rocks, as observed in [22]. The correlation between methane and hydrogen concentration and chromite's modal abundance could also support such hypothesis. Nevertheless, it cannot be excluded that hydrogen and/or methane could also have migrated from other rocks, not flowing directly through the host talc schist. However, it is highly unlikely that methane observed in the chromitites is thermogenic, because no organic matter enriched rocks are found in a 2 km radius from the chromitite body [23]. Furthermore, no metapelites or limestones occur in the underlying metavolcanic stratigraphic units. Hence, migration and preferential storage of thermogenic methane in the chromitites is poorly plausible. Despite that, it is feasible that hydrogen and/or abiotic methane formed during serpentinization of the underlying metabasalts or metakomatiites could have migrated into the chromitites. Still, the low permeability of the metamorphic country rocks and the lack of evident regional fracture zones are limiting constrains to this argument.

Assuming that hydrogen inside the chromitites is autochthonous, larger availability of Cr-spinel surface area for water adsorption is a likely reason why H_2 is abundant in these rocks (as noted by [19]). The combination of high H_2 output in the presence of nickel-rich sulfides and specially Ni-Fe alloys that act as catalysts for Sabatier reaction [20,21] is favorable for in situ methane generation at temperatures over 200 °C. Alternatively, ruthenium-rich minerals [23] may have acted as catalysts for methane synthesis at lower temperatures. In both cases, the required source of CO_2 could have come from the mantle, the atmosphere and, less likely, carbonate rocks. Raman analyses will be necessary to evaluate whether methane is occluded in fluid inclusions, or in widespread microfractures and porous chlorite veins within chromite nodules, as observed by [22].

Abiotic methanogenesis in the Hadean and Archean was likely more productive due to hydrothermal alteration of voluminous Ni-sulfide bearing komatiitic flows and may have influenced the early Earth's atmosphere and temperature [21]. Serpentinized chromium-rich chromitites in greenstone belts could, consequently, represent an additional methane source for the Precambrian atmosphere.

Overall, our results suggest that methane has an abiotic origin, as in chromitites in Greece [22]. However, for a better evaluation of gas origin, including the possibility that some microbially-derived gas formed during weathering, a wider set of bio-geochemical analyses shall be performed. The search for biomarkers [40] and additional indicators of abiotic origin, including the stable C isotope ratio of ethane and propane (as reported in [22]), should help elucidate methanogenesis in the chromitites.

Chlorite Thermometry, Metamorphism and H_2 Generation

As [41] cautioned, empirical chlorite geothermometers are unsatisfactory over a wide range of temperature, chlorite composition and coexisting mineral assemblages. However, these authors estimated that absolute differences between measured and calculated temperatures for the [36] geothermometer vary between 20–150 °C.

Calculated temperatures of the Cedrolina chlorite (inclusions and matrix) cluster around 240–275 °C and are in general good agreement with optimum hydrogen generation conditions during serpentinization of olivine (200–300 °C [18]) even when taking a ±75 °C error into account. Furthermore, the small difference between the applied methods indicates that Fe/(Fe+Mg) is not a first order parameter in the studied samples, presenting always values below 0.12 (Table 2). Finally, the presence of Ni-Fe alloys is characteristic of very low fO_2 conditions and highly reducing geochemical environment [42], suggesting that unconstrained Fe^{3+} should not greatly influence our results.

Assuming that all hydrogen inside the chromitites is autochthonous, chlorite geothermometry should constrain H_2 production and serpentinization at ~250 °C, during retrogression to the greenschist facies. This event postdates the main metamorphic peak and represents one of the latest tectono-metamorphic stages of the Neoproterozoic collage, after which the area was stabilized and cooled to present day conditions. If such is the case, it is reasonable to suppose that latter mixing with carbon dioxide, i.e., methanation, may have taken place during cooling at temperatures below 250 °C. Methane clumped-isotope analyses may reveal, in future, the actual temperature of methane formation [43].

6. Conclusions

Chromitites of the Cedrolina Formation from the Pilar de Goiás greenstone belt in Brazil show methane enrichment, up to 0.31 $\mu g/g_{rock}$. Mineralogical, stratigraphic and stable carbon isotopic data suggest an abiotic origin for CH_4, similar to chromitites studied in Greece [22]. Hydrogen and methane contents seem to be related to high-Cr chromite modal abundance and the presence of nickel sulfides and alloys, which are the most probable catalysts of CO_2 hydrogenation at high temperature (>200 °C) conditions. Accessory ruthenium-bearing minerals in the chromitite [23] could also act as catalysts, especially at lower temperatures (<150 °C). Chlorite geothermometry constrains serpentinization at ~250 °C during retrometamorphism of the lower greenschist facies. Assuming all hydrogen is autochthonous, it is possible to argue that H_2 was formed under similar temperatures. Mixing with CO_2 feasibly occurred under sub-greenschist facies conditions (<250 °C) during cooling and stabilization of the area. We hypothesize, then, that 250 °C represents the upper limit for abiotic methane generation in the Cedrolina chromitites. This retrometamorphic event could be one of the latest stages of the Neoproterozoic collage of the Archean-Paleoproterozoic Terrane of Goiás into the Tocantins Province. The Cedrolina chromitites are the first example of abiotic CH_4 in continental meta-ultramafic rocks related to an Archean-Paleoproterozoic greenstone belt, and imply that serpentinized Cr-rich chromitites could have supplied methane to the early Earth's atmosphere.

Author Contributions: All authors contributed to the project design. Y.d.M.P. conducted the fieldwork, collected the samples, organized the manuscript and, together with F.Z., obtained microprobe data. F.Z. was responsible for chlorite geothermic calculations. G.E. analyzed the samples via planetary ball milling and collected all gas data. All of the authors contributed to the interpretation and discussion of the data, as well as in the writing of the manuscript.

Funding: This research received no external funding.

Acknowledgments: Peter Szatmari is thanked for helpful suggestions and discussions. The authors are grateful to the University Centrum for Applied Geosciences (UCAG) for the access to the E. F. Stumpfl electron microprobe laboratory.

Conflicts of Interest: The authors declare no conflict of interest.

References

1. Thayer, T.P. Serpentinization considered as a constant-volume metasomatic process. *Am. Miner.* **1966**, *51*, 685–710.
2. Etiope, G.; Whiticar, M.J. Abiotic methane in continental ultramafic rock systems: Towards a genetic model. *Appl. Geochem.* **2019**, *102*, 139–152.
3. Wang, D.T.; Reeves, E.P.; McDermott, J.M.; Seewald, J.S.; Ono, S. Clumped isotopologue constraints on the origin of methane at seafloor hot springs. *Geochim. Cosmochim. Acta* **2018**, *223*, 141–158. [CrossRef]
4. McCollom, T.M.; Seewald, J.S. Abiotic synthesis of organic compounds in deep-sea hydrothermal environments. *Chem. Rev.* **2007**, *107*, 382–401. [CrossRef]
5. Marques, J.M.; Etiope, G.; Neves, M.O.; Carreira, P.M.; Rocha, C.; Vance, S.D.; Christensen, L.; Miller, A.Z.; Suzuki, S. Linking serpentinization, hyperalkaline mineral waters and abiotic methane production in continental peridotites: An integrated hydrogeological-bio-geochemical model from the Cabeço de Vide CH_4-rich aquifer (Portugal). *Appl. Geochem.* **2018**, *96*, 287–301.
6. Cipolli, F.; Gambardella, B.; Marini, L.; Ottonello, G.; Vetuschi Zuccolini, M. Geochemistry of high-pH waters from serpentinites of the Gruppo di Voltri (Genova, Italy) and reaction path modeling of CO_2 sequestration in serpentinite aquifers. *Appl. Geochem.* **2004**, *19*, 787–802. [CrossRef]
7. Sherwood Lollar, B.; Westgate, T.D.; Ward, J.A.; Slater, G.F.; Lacrampe-Couloume, G. Abiogenic formation of alkanes in the Earth's crust as a minor source for global hydrocarbon reservoirs. *Nature* **2002**, *416*, 522–524. [CrossRef] [PubMed]
8. Russell, M.J.; Hall, A.J.; Martin, W. Serpentinization as a source of energy at the origin of life. *Geobiology* **2010**, *8*, 355–371. [CrossRef]
9. Tobie, G.; Lunine, J.I.; Sotin, C. Episodic outgassing as the origin of atmospheric methane on Titan. *Nature* **2006**, *440*, 61–64. [CrossRef] [PubMed]
10. Atreya, S.K.; Mahaffy, P.R.; Wong, A.-S. Methane and related trace species on Mars: Origin, loss, implications for life, and habitability. *Planet. Space Sci.* **2007**, *55*, 358–369. [CrossRef]
11. Oehler, D.Z.; Etiope, G. Methane Seepage on Mars: Where to Look and Why. *Astrobiology* **2017**, *17*, 1233–1264. [CrossRef] [PubMed]
12. Szatmari, P. Petroleum Formation by Fischer-Tropsch Synthesis in Plate-Tectonics. *Aapg Bull. Assoc. Pet. Geol.* **1989**, *73*, 989–998.
13. Szatmari, P.; da Fonseca, T.C.O.; Miekeley, N.F. Mantle-like trace element composition of petroleum—Contributions from serpentinizing peridotites. In *Tectonics*; Closson, D., Ed.; InTech: Rijeka, Croatia, 2011; pp. 332–358.
14. Etiope, G.; Schoell, M. Abiotic gas: Atypical, but not rare. *Elements* **2014**, *10*, 291–296. [CrossRef]
15. Etiope, G.; Ionescu, A. Low-temperature catalytic CO_2 hydrogenation with geological quantities of ruthenium: A possible abiotic CH_4 source in chromitite-rich serpentinized rocks. *Geofluids* **2015**, *15*, 438–452. [CrossRef]
16. Etiope, G.; Sherwood Lollar, B. Abiotic methane on earth. *Rev. Geophys.* **2013**, *51*, 276–299. [CrossRef]
17. Klein, F.; Grozeva, N.G.; Seewald, J.S.; McCollom, T.M.; Humphris, S.E.; Moskowitz, B.; Berquó, T.S.; Kahl, W.-A. Fluids in the Crust. Experimental constraints on fluid-rock reactions during incipient serpentinization of harzburgite. *Am. Miner.* **2015**, *100*, 991–1002. [CrossRef]
18. McCollom, T.M.; Klein, F.; Robbins, M.; Moskowitz, B.; Berquó, T.S.; Jöns, N.; Bach, W.; Templeton, A. Temperature trends for reaction rates, hydrogen generation, and partitioning of iron during experimental serpentinization of olivine. *Geochim. Cosmochim. Acta* **2016**, *181*, 175–200. [CrossRef]
19. Mayhew, L.E.; Ellison, E.T.; McCollom, T.M.; Trainor, T.P.; Templeton, A.S. Hydrogen generation from low-temperature water–rock reactions. *Nat. Geosci.* **2013**, *6*, 478–484. [CrossRef]
20. Früh-Green, G.L.; Connolly, J.A.D.; Plas, A.; Kelley, D.S.; Grobéty, B. Serpentinization of Oceanic Peridotites: Implications for Geochemical cycles and Biological Activity. *Subseafloor Biosph. Mid-Ocean Ridges, AGU Geophys. Monogr. Ser.* **2004**, *144*, 119–136.
21. Lazar, C.; McCollom, T.M.; Manning, C.E. Abiogenic methanogenesis during experimental komatiite serpentinization: Implications for the evolution of the early Precambrian atmosphere. *Chem. Geol.* **2012**, *326–327*, 102–112. [CrossRef]
22. Etiope, G.; Ifandi, E.; Nazzari, M.; Procesi, M.; Tsikouras, B.; Ventura, G.; Steele, A.; Tardini, R.; Szatmari, P. Widespread abiotic methane in chromitites. *Sci. Rep.* **2018**, *8*, 8728. [CrossRef]

23. Portella, Y.D.M.; Zaccarini, F.; Luvizotto, G.L.; Garuti, G.; Bakker, R.J.; Angeli, N.; Thalhammer, O. The Cedrolina Chromitite, Goiás State, Brazil: A Metamorphic Puzzle. *Minerals* **2016**, *6*, 91. [CrossRef]
24. Pimentel, M.M.; Fuck, R.A.; Jost, H.; Ferreira Filho, C.F.; Araújo, S.M. The basement of the Brasília Fold Belt and the Goiás Magmatic Arc. In Proceedings of the Tectonic Evolution of South America, 31st International Geological Congress, Rio de Janeiro, Brazil, 6–17 August 2000; pp. 195–229.
25. Jost, H.; Junior, F.C.; Fuck, R.A.; Dussin, I.A.Ô. Uvá Complex, The Oldest Orthogneisses of the Archean-Paleoproterozoic Terrane of Central Brazil. *J. South Am. Earth Sci.* **2013**, *47*, 201–212. [CrossRef]
26. Borges, C.C.A.; Toledo, C.L.B.; Silva, A.M.; Chemale, F.; Jost, H.; de Carvalho Lana, C. Geochemistry and isotopic signatures of metavolcanic and metaplutonic rocks of the Faina and Serra de Santa Rita greenstone belts, Central Brazil: Evidences for a Mesoarchean intraoceanic arc. *Precambrian Res.* **2017**, *292*, 350–377. [CrossRef]
27. Pimentel, M.M.; Jost, H.; Fuck, R.A. O embasamento da Faixa Brasília e o Arco Magmático de Goiás. In *Geologia do Continente Sul-Americano: Evolução da obra de Fernando Fávio Marques de Almeida*; Mantesso-Neto, V., Bartorelli, A., Carneiro, C.D.R., Neves, B.B.B., Eds.; Beca Produções Culturais Ltda: São Paulo, Brazil, 2004; pp. 356–368. (In Portuguese)
28. Jost, H.; Fuck, R.; Brod, J.A.; Dantas, E.L.; Meneses, P.R.; Assad, M.L.; Pimentel, M.M.; Blum, M.L.B.; Silva, A.; Spigolon, A.L.D. Geologia de terrenos Arqueanos e Proterozóicos da região de Crixás-Cedrolina, Goiás. *Rev. Bras. Geociên.* **2001**, *31*, 315–328. (In Portuguese) [CrossRef]
29. Ribeiro Filho, W. Reavaliação da geologia de Pilar-Mara Rosa. In Proceedings of the Anais do I Simpósio de Geologia do Centro-Oeste, Goiânia-GO, Brazil, 25–31 Outubro de 1981; pp. 281–296. (In Portuguese).
30. Jost, H.; De Oliveira, A.M. Stratigraphy of the greenstone belts, Crixás region, Goiás, central Brazil. *J. South Am. Earth Sci.* **1991**, *4*, 201–214. [CrossRef]
31. Jost, H.; Scandolara, J.E. Structural, Petrographic and Geochemical Characteristics of Mafic Dikes Intrusive in Metasedimentary Rocks of the Crixás Greenstone Belt, Goiás. *Geol. USP, Sér. cient.* **2010**, *10*, 119–134. (In Portuguese) [CrossRef]
32. Portella, Y.D.M. Mapeamento Geológico, Caracterização Litoquímica e Potencial Econômico do Corpo de Cromitito de Cedrolina, Santa Terezinha de Goiás-GO. Unpublished Bachelor's Thesis, São Paulo State University (UNESP), Rio Claro, Brazil, 2011. Available online: https://repositorio.unesp.br/handle/11449/120644?locale-attribute=en (accessed on 1 April 2019). (In Portuguese).
33. Lacerda, H. Mapa geológico 1/100.000 do distrito mineiro do Greenstone-Belt de Crixás-Guarinos-Pilar de Goiás (GO). In *Proceedings of the Anais do IV Simpósio de Geologia do Centro-Oeste, Cuiabá-MT, Brazil, 26–31 Outubro de 1997*; Departamento Nacional de Produção Mineral: Goiânia, Brazil, 1997. (In Portuguese)
34. Zaccarini, F.; Portella, Y.D.M.; Bakker, R.J.; Angeli, N.; Garuti, G.; Thalhammer, O.A. Electron microprobe and raman spectroscopic investigation of monazite from chromitites of Cedrolina (Goiás State, Brazil). *Neues Jahrb. fur Mineral. Abhandlungen* **2012**, *189*, 207–215. [CrossRef]
35. Cathelineau, M.; Nieva, D. A chlorite solid solution geothermometer the Los Azufres (Mexico) geothermal system. *Contrib. Miner. Petrol.* **1985**, *91*, 235–244. [CrossRef]
36. Kranidiotis, P.; MacLean, W.H. Systematics of chlorite alteration at the Phelps Dodge massive sulfide deposit, Matagami, Quebec. *Econ. Geol.* **1987**, *82*, 1898–1911. [CrossRef]
37. Cathelineau, M. Cation site occupancy in chlorites and illites as a function of temperature. *Clay Miner.* **1988**, *23*, 471–485. [CrossRef]
38. Zang, W.; Fyfe, W.S. Chloritization of the hydrothermally altered bedrock at the Igarapé Bahia gold deposit, Carajás, Brazil. *Miner. Depos.* **1995**, *30*, 30–38. [CrossRef]
39. Frimmel, H.E. Chlorite Thermometry in the Witwatersrand Basin: Constraints on the Paleoproterozoic Geotherm in the Kaapvaal Craton, South Africa. *J. Geol.* **1997**, *105*, 601–616. [CrossRef]
40. Zwicker, J.; Birgel, D.; Bach, W.; Richoz, S.; Smrzka, D.; Grasemann, B.; Gier, S.; Schleper, C.; Rittmann, S.K.-M.R.; Koşun, E.; et al. Evidence for archaeal methanogenesis within veins at the onshore serpentinite-hosted Chimaera seeps, Turkey. *Chem. Geol.* **2018**, *483*, 567–580. [CrossRef]
41. Caritat, P.D.E.; Hutcheon, I.A.N.; Walshe, J.L. Chlorite geothermometry: A review. *Clays Clay Miner.* **1993**, *41*, 219–239. [CrossRef]

42. Eckstrand, O.R. The Dumont Serpentinite: A Model for Control of Nickel-iferous Opaque Mineral Assemblages by Alteration Reactions in Ultramafic Rocks. *Econ. Geol.* **1975**, *70*, 183–201. [CrossRef]
43. Young, E.D.; Kohl, I.E.; Sherwood Lollar, B.; Etiope, G.; Rumble III, D.; Li, S.; Haghnegahdar, M.A.; Schauble, E.A.; McCain, K.A.; Foustoukos, D.I.; et al. The relative abundances of resolved $^{12}CH_2D_2$ and $^{13}CH_3D$ and mechanisms controlling isotopic bond ordering in abiotic and biotic methane gases. *Geochim. Cosmochim. Acta* **2017**, *203*, 235–264. [CrossRef]

© 2019 by the authors. Licensee MDPI, Basel, Switzerland. This article is an open access article distributed under the terms and conditions of the Creative Commons Attribution (CC BY) license (http://creativecommons.org/licenses/by/4.0/).